Preparation and Optical Characterization of $Yb_3Sb_5O_{12}$: Discussion of Its Suitability for Laser Operation†

Concepción Cascales,*,‡ Carlos Zaldo,‡ and Regino Sáez-Puche§

Instituto de Ciencia de Materiales de Madrid, ICMM, Consejo Superior de Investigaciones Científicas, Cantoblanco, c/Sor Juana Inés de la Cruz, 3, E-28049 Madrid, Spain, and Departamento de Química Inorgánica, Facultad de Ciencias Químicas, Universidad Complutense de Madrid, 28040 Madrid, Spain

Received December 31, 2004. Revised Manuscript Received February 8, 2005

Pure and polycrystalline samples of $Yb_3Sb_5O_{12}$ were prepared under vacuum by solid-state reaction. In this cubic matrix, space group $I\bar{4}3m$ (No. 217), $Z = 4$, Yb^{3+} occupies a single crystallographic site with point symmetry S_4. The confident determination of the Yb^{3+} energy levels was carried out through the analysis of 9 K optical absorption (OA) and photoluminescence (PL) spectra, and 300 K Raman measurements, assisted by models and procedures providing proper estimations of crystal-field (CF) interactions in this host. The parametrization of free-ion and CF effects for Er^{3+} in $Er_3Sb_5O_{12}$ has been revised and then used as reference in the simulation of Yb^{3+} CF energy levels. The correctness of the energy level sequence of Yb^{3+} in $Yb_3Sb_5O_{12}$, which is characterized by a large splitting for the $^2F_{7/2}$ ground state, 933 cm^{-1}, and the composition of the associated wave functions were tested through the successful reproduction of the thermal evolution of the paramagnetic molar susceptibility χ_m of $Yb_3Sb_5O_{12}$. Some parameters of interest accounting for application perspectives as a laser material have been evaluated and compared with those corresponding to other stoichiometric and Yb-doped confirmed laser materials.

Introduction

In recent years trivalent ytterbium Yb^{3+} has attracted great interest as lasant in diode pumped, solid-state laser systems,[1−4] emerging as an alternative to neodymium-based lasers, with some advantages over them: (i) an emission lifetime from three to ten times longer that increases the stored up energy, (ii) a Stokes shift between absorption and emission energies from 3 to 5 times smaller that reduces the thermal energy dissipated to the host, and (iii) a very simple electronic structure, with only one excited state $^2F_{5/2}$, which supposes no losses due to excited-state absorption and up-conversion. Moreover, the lasing efficiency is not reduced by concentration quenching effects, and thus the Yb^{3+} doping level can be very high, allowing a miniaturization of the devices without the PL quenching appearing for most of the highly doped Nd hosts. In addition, the very intense absorption of Yb^{3+} in 980 nm is well-suited to optimize the diode pumping absorption and the sensitization of laser emissions of other rare earths. Yb^{3+} is also used in fundamental academic research, among which the cooling with laser,[5−8] and the optical bistability and hysteresis phenomena,[9−12] are included. The main disadvantage of Yb^{3+} is its quasi-three-level room-temperature operating scheme, which leads to high pumping intensity thresholds for lasing. Using materials possessing a large ground state $^2F_{7/2}$ splitting can overcome this situation. In this case, the system is close to a quasi-four level scheme with easy population inversion and low pumping intensity thresholds. The relationship between the spectroscopic characteristics and laser properties is particularly host-dependent, as this energy level distribution is depending on the crystal-field CF interaction experienced by the Yb in the crystal that has to be as strong as possible for accomplishing the desirable large $^2F_{7/2}$ splitting.

The above reasons have motivated an important search for new Yb-based materials with improved spectroscopic and laser properties with regards to already described materials. But despite the very simple electronic structure of Yb^{3+}, spectral studies of these materials run into the difficulty of unambiguously identifying their Stark levels, mainly due to the strong interaction of Yb^{3+} with the lattice vibrations.[13−17] In fact, the electron−phonon coupling can give rise to intense vibronic sidebands and additional effects such as shifting or

† Dedicated to Prof. Isidoro Rasines, *In Memoriam*.

* To whom correspondence should be addressed. E-mail: ccascales@icmm.csic.es.

‡ Consejo Superior de Investigaciones Científicas.

§ Universidad Complutense de Madrid.

(1) Krupke, W. F. *IEEE J. Sel. Top. Quantum* **2000**, *6*, 1287.
(2) Brenier, A.; Boulon, G. *Europhys. Lett.* **2001**, *55*, 647.
(3) Chénais, S.; Druon, F.; Balembois, F.; Georges, P.; Gaumé, R.; Haumesser, P. H.; Viana, B.; Aka, G. P.; Vivien, D. *J. Opt. Soc. Am. B* **2002**, *19*, 1083.
(4) See *Proceedings of the Scientific Committee of the French Research Group GDR 1148 CNRS: LASMAT Research Group on Laser Materials*, Lyon, France, 14−15 January 2002; Boulon, G., Ed. *Opt. Mater.* **2003**, *22* (2), 81−176.
(5) Fernández, J.; Mendioroz, A.; García, A. J.; Balda, R.; Adam, J. L. *Phys. Rev. B* **2000**, *62*, 3213.
(6) Fernández, J.; Mendioroz, A.; García, A. J.; Balda, R.; Adam, J. L.; Arriandiaga, M. A. *Opt. Mater.* **2001**, *16*, 173.
(7) Epstein, R. I.; Brown, J. J.; Edwards, B. C.; Gibbs, A. *J. Appl. Phys.* **2001**, *90*, 4815.
(8) Bowman, S. R.; Mungan, C. E. *Appl. Phys. B* **2000**, *71*, 807.
(9) Hehlen, M. P.; Kuditcher, A.; Rand, S. C.; Lüthi, S. R. *Phys. Rev. Lett.* **1999**, *82*, 3050.
(10) Kuditcher, A.; Hehlen, M. P.; Florea, C. M.; Winick, K. W.; Rand, S. C. *Phys. Rev. Lett.* **2000**, *84*, 1898.
(11) Redmond, S. M.; Rand, S. C. *Opt. Lett.* **2003**, *28*, 173.
(12) Ciccarello, F.; Napoli, A.; Messina, A.; Lüthi, S. R. *Chem. Phys. Lett.* **2003**, *381*, 163.

10.1021/cm0477063 CCC: $30.25
Published on Web 03/16/2005

splitting of lines in the case of resonant coupling. Moreover, the scarce number of energy levels of the $4f^{13}$ configuration prevents the phenomenological determination of CF parameters describing the CF effects and the subsequent simulation of the Stark levels, even for rather high symmetry point sites. In this context, several ways to facilitate the determination of the energy level diagram of Yb^{3+} materials have been described: more or less semiempirical CF calculation models,[18] the relationship between the maximum CF splitting of the $^4I_{9/2}$ ground manifold of Nd^{3+} and that of $^2F_{7/2}$ Yb^{3+} in the same matrix,[19] and the so-called barycenters law,[18] among others.

From this perspective of exploring new Yb-laser materials, the current work presents the synthesis of the pure polycrystalline stoichiometric antimonate $Yb_3Sb_5O_{12}$ and the CF analysis of its low-temperature optical absorption OA and photoluminescence PL spectra. In the assignment of the Stark levels for Yb^{3+} the possible presence of superimposed vibronic bands has been discussed through the comparison with energies of the lattice phonons observed in the 300 K Raman spectrum. Moreover, the sequence of Yb^{3+} energy levels has been confirmed using predictive methods,[18,19] and CF calculations that optimize the extrapolation to the Yb^{3+} configuration of available CF parameters for various studied R^{3+} ions in the same $R_3Sb_5O_{12}$ host.[20−22] In this context, the parametrization of CF interactions for $Er_3Sb_5O_{12}$ in the true S_4 point symmetry of Er^{3+} has been revised, currently including a larger adjustable number of free-ion interactions. The comparison of the 2−300 K observed paramagnetic molar susceptibility χ_m curve of $Yb_3Sb_5O_{12}$ to the Van Vleck[23]-calculated one using derived wave functions and energy levels offers another way[24−28] to corroborate the diagram of Stark energy levels. Finally, to make a preliminary evaluation of its laser properties, the OA and PL spectra along with the emission lifetime of the $^2F_{5/2}$ multiplet have been measured at 300 K, and values of the absorption and emission cross sections, σ_{EXC} and σ_{EMI}, respectively, saturation intensity I_{SAT} at the pumping wavelength λ_P, and transparency condition β_{MIN} at the laser emission wavelength λ_{EXT} have been derived.

Experimental Section

Synthesis. Analytical-grade mixtures of Yb_2O_3 and Sb_2O_3, pressed and pelletized, have been heated at 963 K under vacuum ($\sim 10^{-3}$ mmHg) in sealed Vycor ampules at 963 K for 7 days and then quenched in liquid N_2.

X-ray Diffraction Analysis. Crystal structure and purity of the sample were tested by X-ray diffraction analysis. The X-ray pattern was collected at room temperature using a Bruker D-8 diffractometer with Cu Kα radiation, scanning in steps of 0.02° 2θ in the angular range of $8 \leq 2\theta \leq 100$, for 4 s each step, and was analyzed by the Rietveld profile refinement method.[29]

Optical Spectroscopy Measurements. The measurement at 300 K of the Raman spectrum was performed with a Renishaw Ramascope 2000 microspectrometer. OA as well as PL spectra measurements were collected in the 9−300 K range on $Yb_3Sb_5O_{12}$ polycrystalline powder dispersed either in KBr or polyethylene thin pellets. The sample temperature was varied using a He close-cycle cryostat connected to a suitable temperature controller. OA spectra were recorded in a Varian Cary 5E spectrophotometer. PL measurements were carried out by exciting the $^2F_{5/2}$ multiplet of Yb^{3+} with a continuous wave Ti-sapphire laser. The PL was dispersed by a SPEX spectrometer ($f = 34$ cm) and measured with a 77 K cooled Ge photodiode. The PL was corrected by the spectral response of the used equipment. The 300 K fluorescence lifetime of the $^2F_{5/2}$ multiplet was measured on $Yb_3Sb_5O_{12}$ dispersed in ethylene glycol, excited with an optical parametric oscillator OPO system, Spectra Physics MOPO-730, and the signal detected after dispersion with a Hamamatsu R2658P photomultiplier and a Lecroy 500 MHz oscilloscope.

Magnetic Measurements. A Quantum Design SQUID magnetometer operating from 2 to 300 K at 1000 Oe was used to perform the magnetic susceptibility measurement. Diamagnetic corrections were calculated with conventional values.[30]

Experimental Results

Synthesis. A slight deficiency (4.8%) of Yb_2O_3 with regards to the stoichiometric amount was required[31,32] to obtain the cubic $Yb_3Sb_5O_{12}$ as a pure phase. Furthermore, to avoid contamination from ytterbium silicate $Yb_2Si_2O_7$,[33] easily formed by the reaction of Yb_2O_3 with silica[34] on the internal surface of the ampule, the pressed pellet was wrapped with gold (99.9%) foil and the capsule placed inside the ampule.

(13) Ellens, A.; Andres, H.; Meijerink, A.; Blasse, G. *Phys. Rev. B* **1997**, *55*, 173. Ellens, A.; Andres, H.; M. L. ter Heerdt, H.; Wegh, R. T.; Meijerink, A.; Blasse, G. *Phys. Rev. B* **1997**, *55*, 180.
(14) DeLoach, L. D.; Payne, S. A.; Kway, W. L.; Tassano, J. B.; Dixit, S. N.; Krupke, W. F. *J. Lumin.* **1994**, *62*, 85.
(15) Lupei, A.; Lupei, V.; Presura, C.; Enaki, V. N.; Petraru, A. *J. Phys.: Condens. Matter* **1999**, *11*, 3769.
(16) Lupei, A.; Aka, G.; Antic Fidancev, E.; Viana, B.; Vivien, D. *J. Lumin.* **2001**, *94−95*, 691.
(17) Montoya, E.; Agulló-Rueda, F.; Manotas, S.; García Solé, J.; Bausá, L. E. *J. Lumin.* **2001**, *94−95*, 701.
(18) Haumesser, P. H.; Gaumé, R.; Viana, B.; Antic-Fidancev, E.; Vivien, D. *J. Phys.: Condens. Matter* **2001**, *13*, 5427.
(19) Auzel, F. *J. Lumin.* **2001**, *93*, 129.
(20) Sáez-Puche, R.; Antic-Fidancev, E.; Lemaitre, M.; Porcher, P.; Cascales, C.; Marcano, C. M.; Rasines, I. *J. Less-Common Met.* **1989**, *148*, 369.
(21) Antic-Fidancev, E.; Cascales, C.; Lemaitre Blaise, M.; Porcher, P.; Sáez-Puche, R.; Rasines, I. *Eur. J. Solid State Inorg. Chem.* **1991**, *28*, 77.
(22) Cascales, C.; Porcher, P.; Sáez Puche, R. *J. Alloys Compd.* **1997**, *250*, 391.
(23) Van Vleck, J. H. *J. Appl. Phys.***1968**, *39*, 365. Van Vleck, J. H. *The Theory of the electric and magnetic susceptibilities*; Oxford University Press: London, 1932.
(24) Jana, Y. M.; Ghosh, M.; Ghosh, D.; Wanklyn, B. M. *J. Magn. Magn. Mater.* **2000**, *210*, 93.
(25) Cascales, C.; Lozano, G.; Zaldo, C.; Porcher, P. *Chem. Phys.* **2000**, *257*, 29.
(26) Hodges, J. A.; Bonville, P.; Forget, A.; Rams, M.; Królas, K.; Dhalenne, G. *J. Phys.: Condens. Mater.* **2001**, *13*, 9301.
(27) Ramakrishnan, S.; Patil, N. G.; Chinchure, A. D.; Marathe, V. R. *Phys. Rev. B 64*, **2001**, 064514.
(28) Binnemans, K.; Malykhina, L.; Mironov, V. S.; Haase, W.; Driesen, K.; Van Deun, R.; Fluyt, L.; Görller-Walrand, C.; Galyametdinov, Y. G. *Chem. Phys. Chem.* **2001**, *11*, 680.
(29) Roisnel, T.; Rodriguez Carvajal, J. WinPLOTR, plotr@llb.saclay.cea.fr, http://www-llb.cea.fr/fullweb/winplotr/winplotr.htm.
(30) Boudreaux, E. A.; Mulay, L. N. *Theory and Applications of Molecular Paramagnetism*; Wiley: New York, 1976; p 494.
(31) Cascales, C.; Marcano, C. M.; Rasines, I.; Fernández, F.; Sáez-Puche, R. *J. Less Common Met.* **1989**, *149*, 63.
(32) Fernández, F.; Sáez-Puche, R.; Cascales, C.; Marcano, C. M.; Rasines, I. *J. Phys. Chem. Solids* **1989**, *50*, 871.
(33) Powder Diffraction File No 82-734. Joint Committee on Powder Diffraction Standards-International Centre for Diffraction Data, PCPDFWIN v.2.2, 2001.
(34) Lee, S. K.; Readey, M. J. *J. Am. Ceram. Soc.* **2002**, *85*, 1435.

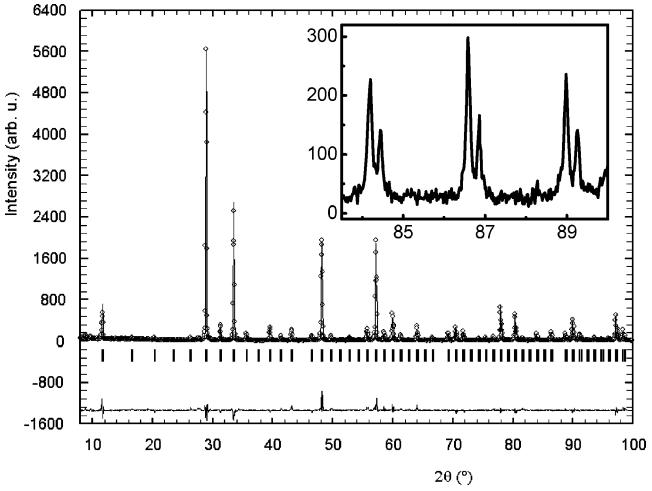

Figure 1. Observed (circles), Rietveld calculated (continuous line), and difference (line at the bottom) X-ray diffraction profiles for $Yb_3Sb_5O_{12}$. The inset shows the $K_{\alpha 1}$ and $K_{\alpha 2}$ contributions in (*7 6 1*), (*8 5 1*), and (*9 3 2*) Bragg peaks, indicating the high crystallinity of the sample.

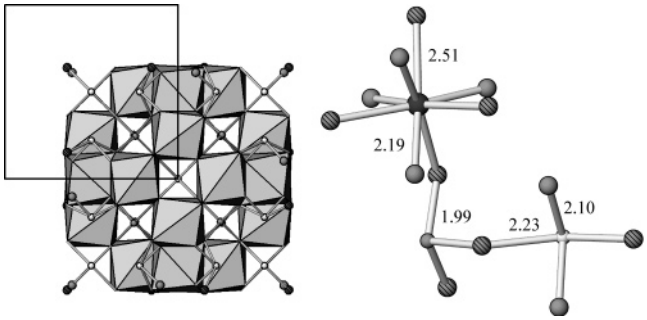

Figure 2. *Left*, the structure of $Yb_3Sb_5O_{12}$ projected in the *ab* plane showing YbO_8 polyhedra and the coordination of Sb(1) (white) and Sb(2) (gray) cations. *Right*, interionic distances around the three cations, gray and striped spheres are the O1 and O2, respectively.

Identification of the Crystal Structure and Its Description. The Rietveld profile analysis was performed in the cubic space group $I\bar{4}3m$ (No. 217), using starting values of the unit cell and positional parameters reported for the isostructural single-crystal $Gd_3Sb_5O_{12}$.[35] The obtained polycrystalline pale orange-yellow $Yb_3Sb_5O_{12}$ sample, with unit cell parameter $a = 10.6764(3)$ Å, was very well crystallized and appeared, to the limits of the technique, completely free of other crystalline phases,[36] see Figure 1.

In $Yb_3Sb_5O_{12}$, Yb^{3+} and Sb^{3+} cations can be imagined as forming a slightly distorted cubic close packing array with oxygens occupying 3/4 of the tetrahedral holes, giving rise to a defect fluorite structure, which can also be related to the Mn_5Si_3 and to the apatite $Ca_5(PO_4)_3(OH)$ structure types.[35] Yb^{3+} ions are located in a quasi-cubic environment of oxygen atoms with S_4 point symmetry, and every YbO_8 polyhedron is sharing its edges with other YbO_8, Figure 2, left, with Yb−Yb distances of 3.77 Å. The two antimony cations, Sb(1) and Sb(2), are coordinated with four and three oxygen atoms, respectively, as shown in Figure 2, right. If the nonbonded electron pairs are considered, they form square and trigonal pyramids, φ-$Sb1O_4$ and φ-$Sb2O_3$, respectively. Main interionic distances for the three polyhedra, in Å, are indicated in Figure 2, right.

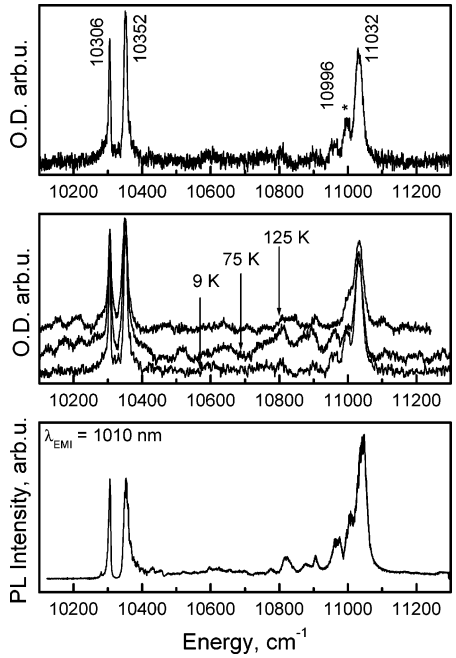

Figure 3. (a) 9 K optical absorption for the $^2F_{7/2} \rightarrow {}^2F_{5/2}$ transition for $Yb_3Sb_5O_{12}$. (b) Comparison of the same OA transition at selected temperatures. (c) 9 K excitation spectrum ($\lambda_{EMI} = 1010$ nm).

Low-Temperature Optical Absorption and Photoluminescence. The S_4 local symmetry of Yb^{3+} in $Yb_3Sb_5O_{12}$ is expected to split its two energy states $^2F_{7/2}$ and $^2F_{5/2}$ into four ($n = 0, 1, 2, 3$) and three ($n' = 0', 1', 2'$) doubly degenerate (Kramers doublets) energy levels, respectively. Figure 3a shows the 9 K OA spectrum of $Yb_3Sb_5O_{12}$ corresponding to the $^2F_{7/2}$ (0) $\rightarrow {}^2F_{5/2}$ (n') transitions. Two sharp and clear lines, at 10306 and 10352 cm^{-1}, can be easily ascribed to $n = 0 \rightarrow n' = 0'$ and $1'$, respectively. Moreover, a complex region in the range 10900−11100 cm^{-1} with a prominent band at 11032 cm^{-1} is observed. Since either multisite character for Yb^{3+} in the $Yb_3Sb_5O_{12}$ matrix or the presence of other crystalline phase in the sample are excluded, the spectrum in this latter region must be due to a mixture of the transition to $^2F_{5/2}$ ($2'$) with vibronic sidebands.

To discard possible contributions from the first excited level of $^2F_{7/2}$, the thermal evolution of these transitions has been further investigated with measurements at 75 and 125 K, and no noticeable change in the intensity of the above peaks has been observed, Figure 3b. The transition peaking at 11032 cm^{-1} has been therefore considered as $^2F_{7/2}$ (0) $\rightarrow {}^2F_{5/2}$ ($2'$).

To obtain additional information, the 9 K excitation spectrum (of the PL shown afterward) has also been recorded. Figure 3c displays the result for an emission wavelength $\lambda_{EMI} = 1010$ nm. Both low-temperature OA and excitation spectra present excellent agreement, giving full confidence to the experimental results.

9 K PL spectra of $Yb_3Sb_5O_{12}$ under different selective excitations corresponding to the energies of the possible $^2F_{5/2}$ levels are presented in Figure 4. The energy difference

(35) Marcano, C. M.; Rasines, I.; Vegas, A.; Otero-Díaz, L. C. *Z. Anorg. Allg. Chem.* **1987**, *555*, 176.
(36) Powder Diffraction File No 79-2117. Joint Committee on Powder Diffraction Standards-International Centre for Diffraction Data, PCP-DFWIN v.2.2, 2001.

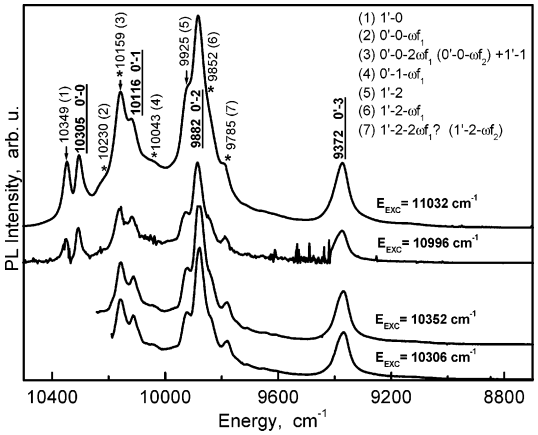

Figure 4. 9 K photoluminescence emission spectra of $Yb_3Sb_5O_{12}$ under different excitations corresponding to the observed peaks in 9 K OA spectra. Arrows indicate transitions from $^2F_{5/2}(1')$, and vibronic sidebands are indicated by asterisks.

($\Delta E = 44$ cm^{-1}) between the two emission bands seen at 10349 and 10305 cm^{-1} in the spectra excited at $E_{EXC} =$ 11032 and 10996 cm^{-1} is nearly the same as that determined from OA measurements between $^2F_{5/2}(0')$ and $^2F_{5/2}(1')$ energy levels, $\Delta E = 46$ cm^{-1}; therefore, the 10349 cm^{-1} PL band corresponds to the emission from $^2F_{5/2}(1')$. This peak structure is also observed in other PL bands of Figure 4, which have been marked with arrows, at 10159 and at 9925 cm^{-1}. Accordingly, the transition that must be taken as reference for the zero-phonon line of $^2F_{5/2}(0') \rightarrow {}^2F_{7/2}(0)$ appears at 10305 cm^{-1}, while the $^2F_{5/2}(0') \rightarrow {}^2F_{7/2}(1, 2, 3)$ emissions are at 10116, 9882, and 9372 cm^{-1}, respectively.

The weak peaks marked by asterisks are considered due to vibronic coupling, as will be explained afterward.

In comparison with most Yb-containing oxide hosts, the previous OA, excitation, and PL spectra show a rather moderate interaction between Yb^{3+} electronic levels and the lattice vibrations in $Yb_3Sb_5O_{12}$. Nevertheless, to discuss the assignment of the above-observed sidebands to electron−phonon couplings, Raman or IR spectra provide the required information on phonon energies. Previously,[37] Raman and IR bands at ∼700 cm^{-1} were attributed to the stretching of the shorter Sb(1)−O(1) bond, and the groups of both Raman and IR bands in the range ∼600−390 cm^{-1} to Sb−O−Sb bridge vibrations, whereas the remaining bands, observed below 350 cm^{-1} but recorded only to 250 cm^{-1}, were indicated to correspond to SbO_2 bending modes and to rare-earth (Yb)−O vibrations. Figure 5 presents the 300 K Raman spectrum recorded for the $Yb_3Sb_5O_{12}$ sample under study, where additional phonons down to 70 cm^{-1} have been recorded. When this spectrum is compared with OA or excitation spectra (normalizing the energy onset to the $^2F_{7/2}(0) \leftrightarrow {}^2F_{5/2}(0')$ zero-phonon line transition), a very similar structure is observed in the 610−710 cm^{-1} region; thus, bands in the low-energy side of the $^2F_{7/2}(0) \rightarrow {}^2F_{5/2}(2')$ transition are due to vibronic coupling.

On the other hand, the bands marked with asterisks in the PL spectra, Figure 4, seem to correspond to the Stokes coupling of some electronic transitions: the emissions

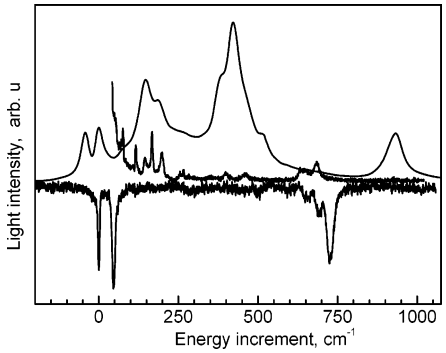

Figure 5. Comparison among the 300 K Raman spectrum (in the center of the figure) and 9 K photoluminescence emission (up-righted) and optical absorption (downward) spectra of $Yb_3Sb_5O_{12}$. The last two spectra have been shifted in energy to consider the origin at the $^2F_{7/2}(0) \leftrightarrow {}^2F_{5/2}(0')$ zero-phonon line transition at 10306 cm^{-1}.

0′−0, 0′−1, and 1′−2 would be coupled with a phonon of ∼75 cm^{-1}, as well as 0′−0 and 1′−2 with two of these phonons, or alternatively with one phonon at 145 cm^{-1}.

From the results derived of the analysis of the above low-temperature OA, excitation, and PL spectra, including the comparison with the Raman spectrum, it is reasonable to consider Yb^{3+} splitting schemes in $Yb_3Sb_5O_{12}$ of 0, 189, 423, and 933 cm^{-1} for the $^2F_{7/2}$ ground multiplet and 10306, 10352, and 11032 cm^{-1} for the $^2F_{5/2}$ excited multiplet.

Crystal Field Analysis and Simulation of the Energy Level Scheme. Considering the limits and difficulties imposed by the described special features of the $4f^{13}$ configuration, some predictive tools are usually utilized to determine the CF potential experienced by Yb^{3+} ions in a given host. Although the interpretation of low-temperature OA and PL spectroscopic data of $Yb_3Sb_5O_{12}$ does not raise important doubts given the moderate electron−phonon interaction, these procedures serve, anyway, to confirm the phenomenological sequence of Yb^{3+} energy levels, and especially the large splitting of its $^2F_{7/2}$ ground state.

The first approach is the use of some calculation model for CF interactions. We applied the well-tested semiempirical Simple Overlap Model (SOM),[38,39] that calculates CF parameters from structural data of the compound. SOM considers effective charges, located around the middle of the Yb^{3+}−oxygen distances, which are assumed to be proportional to the magnitude of the overlap integral, ρ, between the Yb^{3+} and oxygen wave functions. Crystallographic data for $Yb_3Sb_5O_{12}$ were those from our previous X-ray analysis, the effective charge for the oxygen was taken as −1.2, a value which is found not to vary much,[40,41] and ρ was adjusted to a value of 0.06, intermediate between typical values for $4f^N$ configurations, 0.04 (mostly ionic compounds) and 0.08 (mostly covalent compounds). Results of simulated S_4 SOM CF parameters are included in Table 1. After that, the calculation of the sequence of energy levels requires only

(37) Botto, I. L.; Baran, E. J.; Cascales, C.; Rasines, I.; Sáez Puche, R. *J. Phys. Chem. Solids* **1991**, *52*, 431.
(38) Porcher, P.; Couto dos Santos, M.; Malta, O. *Phys. Chem. Chem. Phys.* **1999**, *1*, 397.
(39) Zaldo, C.; Rico, M.; Cascales, C.; Pujol, M. C.; Massons, J.; Aguiló, M.; Diaz, F.; Porcher, P. *J. Phys.: Condens. Matter* **2000**, *12*, 8531.
(40) Morrison, C. A.; Leavitt, R. P. In *Handbook on the Physics and Chemistry of Rare Earths*; Gschneidner, K. A., Jr., Eyring, L., Eds.; North-Holland: Amsterdam, 1982; Vol. 5, p 461.
(41) Alburquerque, R. Q.; Rocha, G. B.; Malta, O. L.; Porcher, P. *Chem. Phys. Lett.* **2000**, *331*, 519.

Table 1. S_4 Simple Overlap Model Simulated (SOM), D_{2d} Extrapolated from the $R_3Sb_5O_{12}$ Series (EX),[20,21] and Phenomenological Sets of CFPs (cm^{-1}) for $Yb_3Sb_5O_{12}$ (D_{2d}) and $Er_3Sb_5O_{12}$ (S_4)

	$Yb_3Sb_5O_{12}$			$Er_3Sb_5O_{12}$
	SOM	EX	D_{2d}[a]	S_4[b]
B_0^2	832	1289	1343(2)	1203(28)
B_0^4	−1281	−1261	−1055(3)	−1544(38)
B_4^4	647	846	880(3)	966(29)
B_0^6	−28	−17	13(13)	−118(30)
B_4^6	1085	585	510(8)	572(24)
S_4^6	−105			131(67)
σ			0.2	13.0
S_2[c]	372	576	600	537
S_4	525	579	544	687
S_6	427	230	200	232
S_T	446	490	482	521

[a] Free-ion parameters (cm^{-1}) for Yb^{3+} in $Yb_3Sb_5O_{12}$: $E^0 = 4748.4(2)$; $\zeta = 2950.2(1)$. [b] Phenomenological free-ion parameters, S_4 fit (cm^{-1}), for Er^{3+} in $Er_3Sb_5O_{12}$: $E^0 = 35006(1)$; $E^1 = 6586.5(9)$; $E^2 = 32.61(2)$; $E^3 = 662.7(1)$; $\alpha = 23.12(5)$; $\beta = -714(4)$; $\gamma = [1790]$; $\zeta = 2372.3(9)$; T2 = [450]; T3 = 51(2); T4 = 116(4); T6 = −134(20); T7 = 178(15); T8 = [350]; $M^0 = 3.7$, $M^2 = 0.56M^0$, $M^4 = 0.32M^0$; $P^2 = 500$, $P^4 = 0.75P^2$, $P^6 = 0.5P^2$. Values between brackets are not varied through the fit of the energy levels. [c] $S_k = \{1/(2k+1)[(B_0^k)^2 + 2(\sum_q[(B_q^k)^2 + (S_q^k)^2]]\}^{1/2}$, $S_T = [(1/3)\sum_k S_k^2]^{1/2}$.

two free-ion parameters, E_0, and the spin−orbit coupling constant ζ, whose variation with the crystal host is theoretically predicted to be weak for a given R^{3+} ion, and consequently can be reasonably taken from the literature.[42]

Another possible approach for the determination of the Yb^{3+} energy levels distribution is the so-called "barycenters plot" method.[18] The model considers that the energy separation between the ground $^2F_{7/2}$ and excited $^2F_{5/2}$ multiplets is constant whatever the matrix, and equal to the spin−orbit splitting for the free-ion, and therefore the energies of both $^2F_{7/2}$ and $^2F_{5/2}$ barycenters present a linear relationship. With our determined energy levels, their barycenters at 386 and 10563 cm^{-1} are well-aligned with this constant energy-separation line, confirming our energy level assignments of the previous section.

A more phenomenological method consists of the evaluation of trends in the variation of CF parameters for the isostructural $R_3Sb_5O_{12}$ series followed for their extrapolation to Yb. D_{2d} CF parameters for R^{3+} = Pr, Nd, Eu, and Er are available[21] and can be used for this purpose. Extrapolated values EX for $Yb_3Sb_5O_{12}$ have been included in Table 1. However, in several R-containing series it has been observed that, besides normal fluctuations of CF parameters, some discontinuity in variation trends is observed toward the middle of the series,[43] Eu^{3+}−Tb^{3+}, and from this point of view, parameters derived from the CF analysis of the low-temperature Er^{3+} optical spectra constitute a very favorable guide to the confirmation of Yb^{3+} energy levels, with clear advantage over Nd^{3+}.[19] The set of adjusted Er^{3+} S_4 CF parameters, for which the D_{2d} ones[21] have been used as starting values, is shown in Table 1. This current S_4 fit, carried out following a previously described procedure,[44] includes, with regards to the previous D_{2d}, a larger number of free-ion interactions, i.e., M^k and P^k integrals, see the bottom of Table 1.

The correct reproduction of the energy level sequences for Pr^{3+}, Nd^{3+}, Eu^{3+}, and currently for Er^{3+} is far to be an isolated consequence of a simple least-squares fitting process, given that for each studied configuration a quite reduced set of CF parameters is considered, which vary smoothly through the series, and their coherence is ensuring the confidence in the simulations of the energy level splittings. Unfortunately, a genuine adjustment is not possible for Yb^{3+} in $Yb_3Sb_5O_{12}$, but in order to attain the precise reproduction of the low temperature observed $^2F_{7/2}$ and $^2F_{5/2}$ manifolds, we carried out the examination of some careful changes in EX and in Er^{3+} CF parameters. Results of optimized D_{2d} Yb^{3+} CF parameters have been included in Table 1.

Simulations of the Stark energy levels for Yb^{3+} have been performed using the program IMAGE,[45] with the indicated sets of CF parameters collected in Table 1: derived from SOM, extrapolated EX, and optimized D_{2d}. In the last case the reproduction of the proposed 0, 189, 423, 933, 10306, 10352, and 11032 cm^{-1} energy levels sequence is excellent, $\sigma = 0.2$ cm^{-1}. It seems that although the oversimplified SOM is able to give a reasonable estimation of CF interactions from crystallographic data, it is more helpful to examine and extrapolate to the Yb^{3+} configuration the tendencies found in the variation of CF parameters along the isostructural $R_3Sb_5O_{12}$ family. In fact, phenomenological CF parameters are closer to those of EX or Er^{3+} sets than to those obtained from the SOM one.

Finally, taking into account that the phenomenological description of the CF is a well-proven tool for the interpretation not only of spectroscopic but also of some magnetic properties in solids,[46] the comparison of the 2−300 K observed paramagnetic molar susceptibility χ_m curve of $Yb_3Sb_5O_{12}$ to the Van Vleck[23]-calculated one, using the phenomenological set of energy levels for $Yb_3Sb_5O_{12}$ and their associated wave functions, offers another way[24−28] to corroborate its diagram of Stark energy levels. This is done using the van Vleck formalism,[23]

$$\chi_i = N\beta^2 \sum_a \left[\frac{\langle \phi_a | (L + g_e S)\mathbf{u} | \phi_a \rangle^2}{kT} - 2\sum_b \frac{\langle \phi_a | (L + g_e S)\mathbf{u} | \phi_b \rangle \langle \phi_b | (L + g_e S)\mathbf{u} | \phi_a \rangle}{E_a - E_b} \right] \times B_a$$

where N is Avogadro's number, β is the Bohr magneton, k is the Boltzmann constant, E and ϕ are the nonperturbed by the magnetic field energy levels and wave functions, respectively, described on the $|SLJM_J\rangle$ basis, $L + g_e S$ is the component (i) of the magnetic interaction associated to a

(42) Carnall, W. T.; Goodman, G. L.; Rajnak, K.; Rana, R. S. *J. Chem. Phys.* **1989**, *90*, 3443.
(43) Lamminmäki, R. J. *The optical properties and simulation of the energy levels of the R^{3+} ions in rare earth oxychlorides.* Ph.D. Thesis, Annales Universitatis Turkuensis, Series A I (Turku University Library, Finland), 1999, Vol. 253.
(44) Rico, M.; Volkov, V.; Cascales, C.; Zaldo, C.; *Chem. Phys.* **2002**, *279*, 73.
(45) Porcher, P. *Fortran routines REEL and IMAGE for simulation of d^N and f^N configurations involving real and complex crystal field parameters*, 1989.
(46) Cascales, C.; Sáez-Puche, R. *Crystal Field and Magnetic Properties, Relationship Between, Encyclopedia of Materials: Science and Technology*; Buschow, K. H. J., Cahn, R. W., Flemings, M. C., Ilschner, B., Kramer, E. J., Mahajan, S., Eds.; Elsevier Science Ltd.: Amsterdam, 2001; pp 1857−1860.

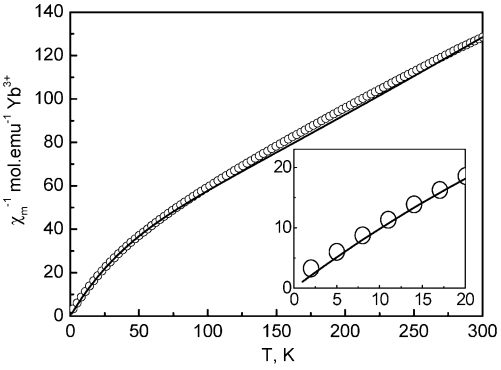

Figure 6. Comparison between experimental (circles) and calculated (line) curves of the thermal variation of χ_m^{-1} for $Yb_3Sb_5O_{12}$.

tensorial operator of rank 1, the magnetic dipole operator, g_e is the gyromagnetic ratio (2.0023), and **u** is the unitary vector corresponding to the *i* axis. The sums run over thermally populated levels, according to the thermal partition law $B_a = [\exp(-E_a/kT)]/[\sum_a \exp(-E_a/kT)]$. The different values of the tensor components, or combinations of them, destroy the isotropy observed for the free-ion or even for an ion in cubic symmetry. The anisotropy components are called $\chi_{||}$ (component 0 of the tensor) and $\chi_\perp$ (components ± 1 of the tensor). The average paramagnetic susceptibility, as measured on a polycrystalline powder, is $\chi_{av} = (2\chi_\perp + \chi_{||})/3 = (\chi_x + \chi_y + \chi_z)/3$. In that expression the matrix elements are calculated using the Racah algebra rules.

The formula is the sum of a temperature-dependent diagonal energy term that normally produces first-order Zeeman splitting and a temperature-independent off-diagonal term, a result of the second-order perturbation, which is reminiscent of the classical Curie−Weiss law. The off-diagonal terms usually have little importance, with the exception of those for Eu^{3+}, with $J = 0$ ground state.

When no kind of magnetic interaction among the magnetic ions is detected, this calculation based on configuration wave functions derived from a CF analysis agrees closely with experimental data, especially for Nd compounds.[46] The calculation of χ and its variation with temperature for the optimized D_{2d} set of CF parameters (with corresponding adjusted free-ion parameters) was also performed using the program IMAGE.[45]

The comparison between experimental and calculated curves of the variation of the χ_m^{-1} with the temperature for $Yb_3Sb_5O_{12}$ is plotted in Figure 6. Above 70 K the experimental χ follows a Curie−Weiss law, $\chi_m^{-1} = 24.9(3) + 0.351(2)$ T mol emu^{-1} ($r = 0.9993$). The effective paramagnetic moment result is 4.7 μ_B, which is very close to the expected value, 4.54 μ_B, for the Yb^{3+} free-ion. The downward deviation from the Curie−Weiss law below 70 K, evident in Figure 6, reflects the splitting of the $^2F_{7/2}$ ground state under the influence of the CF, and the Weiss constant $\theta = -71$ K is entirely due to CF effects, since $Yb_3Sb_5O_{12}$ does not undergo any magnetic exchange interactions.

A very satisfactory concordance is found between observed data and the calculated curve from D_{2d} data. The concordance extends over the entire measured temperature range, the bending at low temperature being especially well-reproduced. From these results we conclude that the correct simulation of the χ vs T curve is proof of obtaining "good wave functions" through "good CF parameters", i.e., those that correctly simulate the observed energy levels of low-temperature OA and PL spectra.

Evaluation of $Yb_3Sb_5O_{12}$ Suitability for Laser Operation. Yb^{3+} in $Yb_3Sb_5O_{12}$ could be considered as a quasi-four-level laser system because of its determined large ground state $^2F_{7/2}$ splitting. To make a first evaluation of the laser quality of this compound, measurements at 300 K of the $^2F_{5/2}$ lifetime as well as OA and PL spectra have been conducted.

Proper $^2F_{5/2}$ lifetime measurements in concentrated Yb systems are difficult because of the self-absorption of the PL and its re-emission, which leads to an artificial time enlargement of light decays. To reduce this effect, a diluted system was used by dispersing $Yb_3Sb_5O_{12}$ in ethylene-glycol ETG. Moreover, the high refractive index of ETG, $n = 1.52$, minimizes inner reflections in the $Yb_3Sb_5O_{12}$ particles. The fluorescence decay measured was non-exponential, exhibiting a short time component of $\approx$15 μs and a long one of $\approx$172 μs. The second lifetime component has a value similar to those observed in other highly concentrated Yb^{3+} systems, 200 μs for $KYb(WO_4)_2$[47] and 183 μs for $LiYb(MoO_4)_2$,[48] whereas it seems probable that the short component should be related to an energy transfer process to the lattice.

The optical absorption coefficient α (cm^{-1}) was measured using a thin pellet of $Yb_3Sb_5O_{12}$ dispersed in polyethylene PET. The effective thickness of $Yb_3Sb_5O_{12}$ in the pellet can be estimated as

$$d_{\text{eff}} = kd \Big/ \left[1 + \frac{\text{PET weight}}{Yb_3Sb_3O_{12}\ \text{weight}} \times \frac{\rho Yb_3Sb_3O_{12}}{\rho \text{PET}}\right]$$

where d is the pellet thickness, ρ is the material density (7.2 g/cm^3 and 0.95 g/cm^3 for $Yb_3Sb_5O_{12}$ and PET, respectively), and k is a factor taking into account the sample preparation (porosity and different plasticity of PET and $Yb_3Sb_5O_{12}$ powder) and high absorption conditions of measurements. This factor was calibrated using a reference sample of $LiYb(MoO_4)_2$. The ground-state absorption cross section of Yb^{3+} $\sigma_{GSA} = \alpha/[Yb]$ can be therefore obtained taking into account the Yb density of the $Yb_3Sb_5O_{12}$ compound, $[Yb] = 9.86 \times 10^{21}$ cm^{-3}. Figure 7 shows the obtained result.

The emission cross section, σ_{EMI}, is calculated by the reciprocity principle[49] as

$$\sigma_{EMI}(E) = \sigma_{GSA}(E) \times (Z_l/Z_u) \times \exp[(E_{zl} - E)/k_BT]$$

where E_{zl} is the energy gap between the lowest Stark levels of the $^2F_{5/2}$ and $^2F_{7/2}$ multiplets, E is the light energy, Z_l and Z_u are the partition functions of the lower and upper multiplets, $Z_i = \sum_i d_i \exp(-E_i/k_BT)$ being $d_i = 2$ due to the Kramers degeneracy. With the energy position E_i of the Yb^{3+} levels in the ground and excited multiplets discussed previously, we arrive at $Z_l/Z_u = 0.846$. Figure 7 also shows a

(47) Pujol, M. C.; Bursukova, M. A.; Güell, F.; Mateos, X.; Solé, R.; Gavaldá, J.; Aguiló, M.; Massons, J.; Díaz, F.; Klopp, P.; Griebner, U.; Petrov, V. *Phys. Rev. B* **2002**, *65*, 165121.
(48) Volkov, V.; Cascales, C.; Kling, A.; Zaldo, C. *Chem. Mater*. **2005**, *17*, 291.
(49) McCumber D. E. *Phys. Rev*. **1964**, *136*, A954.

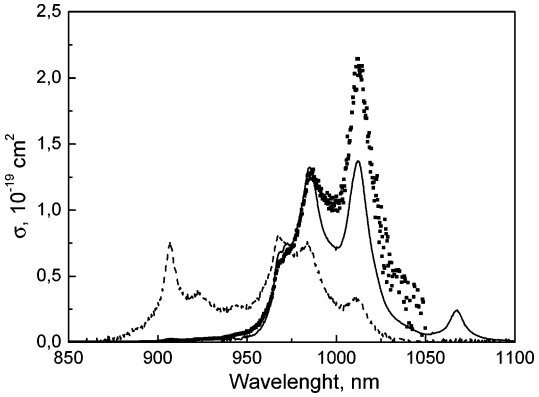

Figure 7. 300 K cross sections of $Yb_3Sb_5O_{12}$. Experimental ground-state absorption cross section σ_{GSA} (dashed line). Calculated emission cross section σ_{EMI}-RM (points). Normalized experimental emission cross section σ_{EMI} (solid line).

comparison between the calculated and experimental values of σ_{EMI}. For this purpose the experimental PL spectrum was normalized to the calculated emission cross section at the zero-phonon line absorption (~970 nm). σ_{EMI} values calculated for $\lambda > 1050$ nm have been ignored because of the large uncertainty of the OA measurements in this range, and in fact, σ_{EMI} calculated values are slightly overestimated due to the actually nonconstant spectral behavior of k. Nevertheless, the correlation between experimental and calculated emission spectral distributions is very satisfactory considering the inherent uncertainty for optical absorption measurements using polycrystalline powder materials.

The fraction of excited Yb ions in a laser experiment is given by the ratio between the absorbed intensity I_{ABS} and the saturation intensity, I_{SAT},[50] and therefore low I_{SAT} values are desired. I_{SAT} is given by

$$I_{SAT} = hc/(\lambda_{EXC} \cdot \sigma_{EXC} \cdot \tau)$$

where σ_{EXC} is the absorption cross section at the excitation wavelength, λ_{EXC}, and τ is the emission lifetime of the $^2F_{5/2}$ multiplet. Two pumping wavelengths with similar absorption cross sections of $\sigma_{EXC} = 8.1 \times 10^{-20}$ cm^2 can be considered: $\lambda_{EXC} \approx 907$ nm and $\lambda_{EXC} \approx 967$ nm. Taking now $\tau = 172$ μs as representative of the intrinsic $^2F_{5/2}$ fluorescence of Yb^{3+} in $Yb_3Sb_5O_{12}$, the saturation intensity is $I_{SAT} \approx 14$ kW/cm^2. This value is within the $I_{SAT} = 5-30$ kW/cm^2 range calculated for Yb^{3+} in several oxide and fluoride laser hosts.[50]

(50) DeLoach, L. D.; Payne, S. A.; Chase, L. L.; Smith, K. L.; Kway, W. L.; Krupke, W. F. *IEEE J. Quantum Electron.* **1993**, *29*, 1179.

Another relevant laser parameter is given by the transparency condition at the laser emission wavelength λ_{EXT}

$$\beta_{MIN} = \frac{\sigma_{ABS}(\lambda_{EXT})}{\sigma_{EMI}(\lambda_{EXT}) + \sigma_{ABS}(\lambda_{EXT})}$$

At $\lambda_{EXT} \approx 1067$ nm, $\sigma_{ABS} \approx 0.2 \times 10^{-20}$ cm^2 and $\sigma_{EMI} = 2.8 \times 10^{-20}$ cm^2, and therefore $\beta_{MIN} = 0.07$, a value which is similar to those shown by well-tested Yb laser hosts.[50] From this point of view and owing to the large crystal field splitting of $^2F_{7/2}$, $Yb_3Sb_5O_{12}$ exhibits a favorable situation for lasing around $\lambda_{EXT} \approx 1067$ nm.

Conclusions

Stoichiometric incorporation of Yb^{3+} in the 8-fold S_4 point site of the cubic lattice $R_3Sb_5O_{12}$ host has been demonstrated to produce strong local CF effects, leading to a very large $^2F_{7/2}$ ground-state splitting, which is in principle necessary to obtain a quasi-four-level laser operating scheme. Only rather moderate interaction with the lattice vibrations is affecting the electronic transitions in $Yb_3Sb_5O_{12}$. The confident assignment of energy levels results from careful evaluations of low-temperature OA and PL spectra and comparison with energies of the lattice phonons, combined and confirmed with the assistance of procedures providing suitable estimations of the CF effects in the matrix. The correct simulation of the variation with the temperature of the paramagnetic susceptibility of this compound independently verifies the composition of wave functions associated with the proposed scheme of energy levels for $Yb_3Sb_5O_{12}$. The perspectives for laser emission around $\lambda_{EXT} \approx 1067$ nm seems to be favorable. The I_{SAT} value obtained is relatively large and suggests that ways to reduce it should be explored. This can be likely achieved by reducing the Yb concentration in the crystal, for instance, through the preparation of mixed Y/Yb or Lu/Yb compositions, since in this way Yb−Yb interactions should decrease and the fluorescence lifetime will be expected to increase.

Acknowledgment. The authors acknowledge the support from the Spanish projects MAT2002-04603-C05-05, MAT2001-1430, and CAM MAT/0434/2004.

Supporting Information Available: Additional table with 10 K observed and S_4 calculated energy levels of Er^{3+} in $Er_3Sb_5O_{12}$ (PDF). This material is available free of charge via the Internet at http://pubs.acs.org.

CM0477063